Network Analysis of Brain Activity during Processing of Natural Human Interaction

Markus Ferdinand Dablander

UCL CoMPLEX MRes Project Report 2

Project Supervisors:

Dr. Jeremy Skipper
University College London

Dr. Lewis Griffin
University College London

April 6, 2017

Abstract

We explore a network-based analysis method of fMRI-data obtained from an individual watching a television show containing a variety of forms of natural human communication and interaction. The fMRI activity time series of the individual is decomposed using *temporal independent component analysis*; each temporal independent component (tIC) is then associated with a region of the brain. Using data from the *neurosynth* database, each tIC is labeled with one anatomical and one functional term connected to activity in the corresponding brain area.

In a next step, each tIC is identified with the labeled node of a network graph G. In this graph, there is a directed edge from tIC x_i to tIC x_j if there is a significant cross-correlation between the activity time series of x_i and x_j. To compute a p-value for each cross-correlation value, an empirical null distribution is created by applying a block-bootstrapping method to the available time series data. The false discovery rate is controlled with the Benjamini-Hochberg-Yekutieli procedure.

Topological properties of G are studied by comparing values of structural descriptors with null distributions generated via simulations of equivalent random networks. In addition, the structure of G is interpreted in a biological context.

Contents

1 Introduction: The Brain as an Interdependent Network **3**

2 Method **5**
2.1 Experiment 5
2.2 Temporal Independent Component Analysis 5
2.3 Labeling of Independent Components 6
2.4 Computation of Significant Cross-Correlation Values 7
2.4.1 Cross-Correlation 7
2.4.2 Block Bootstrapping to Create Uncorrelated Time Series 9
2.4.3 The Benjamini-Hochberg-Yekutieli Procedure 11

3 Brain Network Analysis **13**
3.1 Network Structure 13
3.2 Interpretation 17
3.3 Further Thoughts 19

4 Appendixes **21**
4.1 A: Imaging Technique 21
4.2 B: Data Preprocessing before ICA 21
4.3 C: List of 77 Weighted Edges of G 21

Word Count: 6375.

1 Introduction: The Brain as an Interdependent Network

One of the key challenges of cognitive neuroscience is to gain a theoretical understanding of the way the brain supports many of the highly general and unspecific functions that are required in everyday life. Many complex cognitive processes that are performed in a natural environment consist of a wide range of subprocesses that can be associated with activity in different regions of the brain. These subprocesses constantly need to be coordinated and well-orchestrated by the mind in order to give rise to flexible and sophisticated patterns of behaviour. The process of interpersonal communication, for example, can be broken down into language comprehension, face recognition, memory etc. To make these functions work together, the brain needs to control the hierarchy and information flow between those subprocesses while at the same time interpreting and integrating contextual information from the environment.

This implies that the cognitive mechanisms behind tasks like real-world human communication cannot be fully understood by studying the brains response to highly specific stimuli in artifical environments; these stimuli are likely to only produce activity in a small set of subprocesses. In order to get an appropriate picture of real-world cognitive processing, one has to not only understand the isolated subprocesses involved in performing a complex task, but also the way how these subprocesses interact in the brain in normal conditions.

Network theory provides an appropriate formal framework for studying the interactions of different entities within a system and is therefore well-suited for modelling the dependency structure of subprocesses in the brains of individuals that are exposed to natural stimuli. In many cases, a view on the brain as a network of interdependent substructures can overcome theoretical problems and shortcomings that arrise when trying to explain the adaptability of complex mental functions with classical models that do not put enough emphasis on the interactions between distinct subprocesses.

Skipper [2015] [12], for example, has presented a new network-based model of neuronal language organization (NOLB), that can, among other things, explain how the brain can overcome the problem of ambiguity in language comprehension by making constant use of contextual information.

Van den Heuvel et al. [2009] [14] have emphasized that functional networks in the resting-state brain tend to both show a high clustering coefficient and a small average path length (*small-world networks*). When performing group analysis on a set on individuals, they could detect a strong negative association between IQ and average path length in the individuals functional brain network. It seems reasonable to assume that shorter path lengths facilitate communication and interaction between brain areas which might have a beneficial effect on an individuals intellectual capabilities.

Bassett et. al. [2013] [1] derived a time-evolving neural network based on correlated activity among a wide range of brain regions in individuals learning a new motor skill. They detected a core-periphery structure within this network

and could link certain structural differences in individuals (namely a better separation between core and periphery) to a better learning outcome.

These examples illustrate the importance of understanding the interdependence structure of large-scale neural networks to gain an appropriate understanding about the working mechanisms of the mind in natural situations.

The goal of this project is to explore a network-based analysis method of fMRI-data from an individual watching a television show that contains real-life human communication and interaction. We apply *temporal independent component analysis* to deconstruct the fMRI activity time series of the individual into parts; each temporal independent component (tIC) can be linked to a particular brain region. This fact is used to interpret every tIC as a cognitive subprocess and label it with data from the *neurosynth* database.

We then identify each tIC with the labeled node of a network graph and construct directed, weighted edge from tIC x_i to tIC x_j if and only if there is a significant cross-correlation between the activation time series of x_i and x_j. A time lag of $\tau = 3$ time points (4.5 seconds) is chosen for the cross-correlation; the weights of edges are given by the cross-correlation values and the directions of edges indicate the flow of time. We use `Python` to apply a block-bootstrapping method to the fMRI data in order to derive a null distribution $\hat{F}_0$ for the correlation values of uncorrelated fMRI activity time series. This distribution can then be used to assign p-values to our edges. The Benjamini-Hochberg-Yekutieli procedure is used to keep the expected false discovery rate below a level of $\alpha = 0.4$.

The resulting network G can be studied to obtain structural insights into the time-shifted linear dependency structure between different neural functions involved in the processing of a natural stimulus. We use `Wolfram Mathematica` simulate a total number of 100 000 equivalent random networks and derive null distributions for the number of weakly connected components, the number of self-loops, the number of hubs, the clustering coefficient of the biggest weakly connected component as well as the average weak path length of the biggest weakly connected component. These null distributions are then compared to the corresponding features of G to detect special characteristics. We conclude with a short discussion of possible biological interpretations of the findinds and further research questions.

2 Method

2.1 Experiment

The individual participating in the study was a right-handed native English speaker with normal hearing and vision ability and no history of psychiatric or neurological illness. The individual provided written informed consent and the study was approved by the Institutional Review Board (IRB) of Weill-Cornell Medical College.

The participant watched and listened to 32 minutes and 24 seconds of an episode of the television game show *Are You Smarter Than A 5th Grader?* (season 2, episode 24, aired 02/07/2008). The episode was edited down from its original length (without changing understandability) and was shown in six segments. Each segment was followed by a short break for the participant. One reason for the choice of this specific show was that it contains several natural audiovisual dialogue sequences between host, contestant and six other peripheral individuals.

During the experiment, a 3 Tesla MR scanner (GE Medical Systems, Milwaukee, WI) was used for brain imaging. There were six consecutive functional runs, each run for one segment of the television game show (durations [m : s]: 05:36, 05:45, 05:42, 05:42, 04:51, 05:51).

Further details of the imaging technique can be found in appendix A.

2.2 Temporal Independent Component Analysis

The `AFNI` software package (Cox [1996] [6]) was used to preprocess the initial data. Among other things, this preprocessing step included removal of artifacts, removal of voxels outside the participants brain as well as concatenation of the data of all segments. The result was one long multidimensional signal T of length $l := 1302$, where two time points are separated a real time of 1.5 seconds. Each component of T consists of the activation time series of a voxel in the participants brain. Further details on the preprocessing procedure can be found in appendix B.

Next, the `R` package `AnalyzeFMRI` was used to perform *fast temporal independent component analysis* with T. This delivered a total number of $m := 315$ independent components $I := \{x_1, ..., x_m\}$. Each tIC x_i has the form of a row vector that describes an fMRI activity time series:

$$x_i = (x_{i,1}, ..., x_{i,l}).$$

The initial part of the activity time series x_1 is depicted in figure 1.

The components of T can be approximated by linear combinations of elements in $\{x_1, ..., x_m\}$.

In this study, we focussed only on the first $n := 50$ independent components,

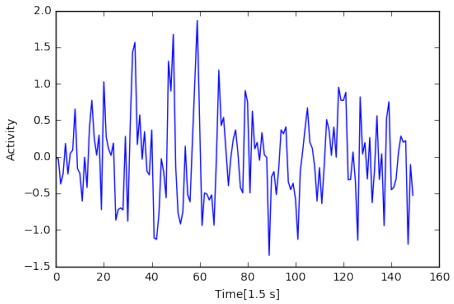

Figure 1: Activity time series of temporal independent component (`Python`).

collected in the $n \times l$ matrix

$$X := \begin{pmatrix} x_1 \\ \vdots \\ x_n \end{pmatrix}.$$

Observation of the data has shown a much stronger linear dependence among the first independent components in comparison to the full set $\{x_1, .., x_{315}\}$. In particular, components $x_{51}, ..., x_{315}$ seemed to have almost no linear dependence structure at all; including them in our analysis would have added a disproportionate amount of noise to the significance analyis performed below. In contrast to other signal decomposition methods like principal component analysis, the components produced by ICA-algorithms generally do not come with any natural ordering. The *fast* independent component analysis algorithm (Hyvrinen [2000] [10]), however, works sequentially and extracts one component at a time while taking already extracted components into account. It is possible that this sequential working mechanism is responsible for the observed bias in linear dependency.

An in-depth discussion of the used ICA algorithm and its applications to fMRI time series can be found in the article of Bordier et. al. [2011] [5].

2.3 Labeling of Independent Components

The structure of each x_i could be used to link it to a particular region in the brain. The activity time series of an x_i was then interpreted as the activity time series of the anatomical brain parts and cognitive subprocesses linked to this brain region. To find the anatomical parts and cognitive subprocesses corresponding to our brain regions, we compared each brain map with data from the *neurosynth* database [1]. A detailed description how to use and interpret the data available in the neurosynth database can be found in the Nature Methods paper by Yarkoni et. al. [2011] [15].

[1] www.neurosynth.org

For each tIC x_i, we used *neurosynth*-data to generate correlation strengths between x_i and a wide range of labels. We then divided this set of labels into two lists: a list of 235 anatomical terms (*primary motor, motor cortex, somatosensory, superior temporal, ...*) and a list of 199 functional terms (*acoustic, abstract, social, speech production, visual, ...*). Meaningless labels that did not fit into either category were deleted. Finally, we double-labeled each x_i with both its top anatomical and its top functional term.

Since the tIC in X are constructed to correspond to maximally independent temporal processes within our fMRI data, the overlap between the brain areas associated with two different tIC x_i and x_j is generally small; therefore, the functional and anatomical terms associated with x_i and x_j are usually sufficiently different to create an interesting structure.

2.4 Computation of Significant Cross-Correlation Values

2.4.1 Cross-Correlation

To now construct a network, every labeled tIC is identified with a node in. Since every tIC $i \in \{1, ..., n\}$ is characterized by its own one-dimensional activation time series,

$$x_i = (x_{i,1}, ..., x_{i,l}),$$

we can compute the *cross-correlation values* $\text{corr}(x_i, x_j, \tau)$ between all $n^2 = 2500$ possible edges (x_i, x_j). We define

$$\mu(x_i) := \frac{1}{l} \sum_{k=1}^{l} x_{i,k},$$

$$\sigma(x_i) := \sqrt{\frac{1}{l} \sum_{k=1}^{l} (x_{i,k} - \mu(x_i))^2},$$

and

$$x_{i,[k:r]} := (x_{i,k}, ..., x_{i,r}).$$

Then

$$\text{corr}(x_i, x_j, \tau) := \frac{\sum_{k=1}^{l-\tau} (x_{i,k} - \mu(x_{i,[1:l-\tau]}))(x_{j,\tau+k} - \mu(x_{j,[\tau+1:l]}))}{\sigma(x_{i,[1:l-\tau]})\sigma(x_{j,[\tau+1:l]})},$$

$$\tau \in \{0, ..., l-2\}.$$

For $\tau = 0$, this is exactly the Pearson correlation coefficient between x_i and x_j.

For $\tau > 0$, it is the correlation coefficient of the first $l - \tau$ values of x_i and the last $l - \tau$ values of x_j. This corresponds to a time-shift, where x_i happens τ time steps before x_j.

In our study, we chose a time shift of $\tau := 3$ (= 4.5 seconds). Observation of the data has shown that this shift is big enough to avoid inaccuracies due to the limited time resolution of the fMRI data, but still small enough to allow the existence of an interesting dependence structure. This time lag shortens the length of all x_1,...,x_n from $l = 1302$ to $l_\tau := l - \tau = 1299$.

The value of $\text{corr}(x_i, x_j, \tau)$ can be seen as the weight of a directed edge from node x_i to node x_j in our network. Since the cross-correlation function is not symmetric (in general $\text{corr}(x_i, x_j, \tau) \neq \text{corr}(x_j, x_i, \tau)$), our edges need to be directed (with the direction indicating the flow of time).

Since we have $n = 50$ nodes and since we allow self-loops, we can use the cross-correlation function to get a total number of $50^2 = 2500$ potential edges and associated correlation values. It would not be smart, however, to take all these edges into account when constructing our network; many of our cross-correlation values might just be the result of chance and the underlying pairs of time series might in fact be uncorrelated. But how can we make a good guess which of our values reflect an actual linear dependence between a pair of time series?

To tackle this problem, we need to assign a p-value $p_{i,j}$ to each correlation value $\text{corr}(x_i, x_j, \tau)$. Let us assume that

$$Y_1 = (Y_{1,1}, ..., Y_{1,l_\tau})$$

and

$$Y_2 = (Y_{2,1}, ..., Y_{2,l_\tau})$$

are two identically distributed stochastic processes that model tIC activity time series of length l_τ. Furthermore, let us assume that we can expect Y_1 and Y_2 to be uncorrelated:

$$\text{E}(\text{corr}(Y_1, Y_2, 0)) = 0.$$

Then we can define the cumulative distribution function of the random variable $K_0 := |\text{corr}(Y_1, Y_2, 0)|$ via

$$F_0(t) := \text{P}(K_0 \leq t)$$

and the p-value for each cross-correlation value $\text{corr}(x_i, x_j, \tau)$ as

$$p_{i,j} := \text{P}(K_0 \geq |\text{corr}(x_i, x_j, \tau)|) = 1 - F_0(\text{corr}(x_i, x_j, \tau)).$$

So the p-value of edge (x_i, x_j) describes the probability of getting an edge weight that is at least as extreme (in absolute value) as the observed edge weight under the null hypothesis that there is no cross-correlation between the two underlying time series. But how can we find the distribution of K_0?

2.4.2 Block Bootstrapping to Create Uncorrelated Time Series

If we had a large set of realizations I_0 of random variables $Y_1, Y_2, ...$ with the above properties and the right length l_τ, then we could correlate the elements in I_0 to simulate realizations of K_0 and collect the correlation values in a set R_0. This set R_0 could then be used to create an empirical estimate $\hat{F}_0$ of F_0.

Of course we cannot just use our data set $I = \{x_1, ..., x_m\}$ with $m = 315$ to generate realizations of K_0, since some of the tIC activity time series in I might in fact be correlated. What we can do, however, is to use I to artificially create time series that (at least approximately) look like realizations of the above stochastic processes Y_1, Y_2 by applying a *block bootstrapping method*. These artificial time series can then be cut to the right length and correlated to create values that look like realizations of K_0.

We start by decomposing every time series x_i of full length $l = 1302$ into a sequence of blocks of the same length. For block length $l_b \in \{1, ..., l\}$, this gives us a number of $\max\{k \in \mathbb{Z} \mid k \leq \frac{l}{l_b}\} := s$ blocks. The first l_b values of x_i form the first block $a_{i,1}$, the second l_b values form the second block $a_{i,2}$; proceeding like this, we can write

$$x_i = (a_{i,1}, ..., a_{i,s}, a_{i,s+1}).$$

Here $a_{i,1}, ..., a_{i,s}$ are big blocks of length l_b and $a_{i,s+1}$ is a small block of length $\in \{0, ..., l_b - 1\}$.

Now we collect all big blocks and all small blocks of all m time series contained in I in two sets:

$$B_{\text{big}} := \bigcup_{i=1}^{m} \{a_{i,1}, ..., a_{i,s}\}, \qquad B_{\text{small}} := \bigcup_{i=1}^{m} \{a_{i,s+1}\}.$$

Since it is highly unlikely that two blocks will be the same, the set B_{big} now contains sm big blocks and the set B_{small} contains m small blocks. These two sets can be used to construct new time series of length $l = 1302$. To do this, we draw s big blocks out of B_{big} and 1 small block out of B_{small} (without replacement) and then put these $s+1$ blocks together in random order to produce a new time series of the form

$$y = (a_{i_1,j_1}, ..., a_{i_{s+1},j_{s+1}})$$

Due to the random ordering of blocks, it is also possible for the small block to appear somewhere in the middle of the new time series.

We can repeat this procedure m times before we run out of blocks. In the process, we produce a new set of time series

$$I_0 := \{y_1, ..., y_n\}.$$

Each y_i can be cut off to a length of l_τ and consists of blocks of values from our original data set I. It therefore inherits a great part of the autocorrelation structure of typical fMRI activation time series for a sufficiently large block length

l_b. At the same time, the mixing of the data that is caused by the block decomposition and reordering destroys almost the entire correlation structure between different series that show linear dependence. [2] Therefore, the set I_0 can be seen as a set of approximations of realizations of random variables $Y_1, Y_2, ...$ with the properties from above and we can correlate the time series in I_0 to create a set of null values R_0 from which we can extract our estimated distribution $\hat{F}_0$ for K_0. Since we can produce as many different sets R_0 as we want by repeating the above procedure, we can also generate an arbitrary number of values in R_0; the more values, the smoother our estimate $\hat{F}_0$ for F_0 becomes.

Computational Test. To further legitimate our simulation strategy, we can first construct an empirical distribution $\hat{F}_0$ with time series of length 1000 and then compare $\hat{F}_0$ with cross-correlation values obtained from our initial data set I and a massive time lag $T = 302$. If $T >> 0$, then we can assume, that the compared time series are largely uncorrelated but still have the autocorrelation structure of fMRI activation time series. If we choose a time lag of $T = 302$, then we effectively correlate independent time series of length $l - T = 1302 - 302 = 1000$ and if we compare all possible pairs of different series, we get $m(m-1) = 98910$ values

$$C_T = \{c_{T,1}, ..., c_{T,98910}\}.$$

The values in C_T can again be seen as realizations of the random variable K_0 (for a time series length of 1000). We can now use the *Kolmogorov-Smirnov test* to decide whether C_T was drawn from our artificial distribution $\hat{F}_0$. Here, $\hat{F}_0$ was produced by defining a block length of $l_b = 100$, repeating our bootstrapping method 100 times (and creating $\frac{315*314*100}{2} = 4\ 945\ 500$ artificial values in the process) and cutting the mixed time series off to a length of 1000.

Applying the Kolmogorov-Smirnov test delivers a p-value of 0.4897. Despite our big sample size of nearly 100 000 values, we cannot reject the null hypothesis that $C_{0,\tilde{\tau}}$ was drawn from the distribution $\hat{F}_0$. This shows that we can be reasonably confident that our method actually does what it is intended to do: simulate uncorrelated fMRI activity time series of independent components.

Why did we not use the empirical distribution obtained by comparing time series with big time lags immediately instead of doing all the work of implementing a bootstrapping algorithm? The distribution of C_T is dependent on T and if T is too small, then the time series we want to correlate become dependent again. The advantage of our artificial method is the fact that we can control the length of the uncorrelated time series that are generated. In particular, with the block bootstrapping approach we can simulate *uncorrelated* fMRI activation time series of length $l_\tau = 1299$, which is relevant for us since we chose a time lag of $\tau = 3$ for our study and the total length of the series in our data set is

[2] It could still happen that two blocks of highly correlated time series appear again parallel to each other in two new, mixed time series y_i and y_j and increase the correlation value; due to the huge amount of mixing possibilities for our blocks, however, this effect is negligible.

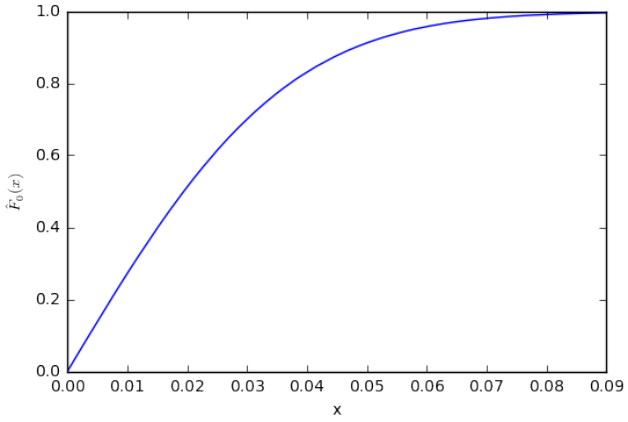

Figure 2: Empirical distribution $\hat{F}_0$, constructed from 14 836 500 realizations of K_0 (`Python`).

$l = 1302$. Because of the correlation structure in our data for small time lags, estimating F_0 for a time series length of $l_\tau = 1299$ would not be possible by just getting the empirical distribution of correlation values from tIC in I obtained with a time lag of $\tau = 3$.

In this project, we created a reasonably smooth cumulative empirical distribution $\hat{F}_0$ by using our $m = 315$ time series in I to create 300 different sets I_0 of time series of length $l_\tau = 1299$ and block size $l_b = 100$. Since each set I_0 can be used to create $315 * 314/2 = 49\ 455$ values, our set R_0 of simulated realizations of K_0 contained $49\ 455 * 300 = 14\ 836\ 500$ elements. $\hat{F}_0$ is depicted in figure 2.

2.4.3 The Benjamini-Hochberg-Yekutieli Procedure

After the construction $\hat{F}_0$ from C_0 and the computation of p-values $p_{i,j}$ for all cross-correlation values $\text{corr}(x_i, x_j, 4)$, the next step is to go through all pairs (x_i, x_j) and reject the null hypothesis that x_i and x_j are uncorrelated if $p_{i,j}$ is sufficiently small. But what does *sufficiently small* mean?

Let us assume that we just reject every edge (x_i, x_j) with a p-value $p_{i,j} < 0.05$. Furthermore, let us assume that for a time lag of $\tau = 3$, a total number of 99 % of the pairs (x_i, x_j) are uncorrelated and 1 % have some underlying linear dependence. In total we can produce $n^2 = 2500$ cross correlation values with our data in X. Then we can expect to still discover around $2500 * 0.99 * 0.05 = 123.75$ false "significant" cross-correlation values among the uncorrelated pairs. Even if we are optimistic and assume that we can find all the $2500 * 0.01 = 25$ pairs that are actually correlated, we have in total detected about 148.75 significant pairs, but more than 80 % of them are false discoveries.

The *Benjamini-Hochberg-Yekutieli procedure* offers a simple solution to the problem of controlling the false discovery rate in a large series of statistical tests.

Let us consider a set of null hypothesis

$$H_1, ..., H_m$$

with associated p-values

$$p_1, ..., p_m.$$

W.l.o.g. we can assume that these p-values are ordered according to size:

$$p_1 < ... < p_m.$$

We now define a threshold function

$$t : \mathbb{N} \times \mathbb{N} \times [0, 1] \to \mathbb{R}$$

$$t(k, m, \alpha) = \frac{k\alpha}{m \sum_{i=1}^{m} \frac{1}{i}}.$$

as well as a threshold index

$$k_{max}(m, \alpha) := \max\{k \in \{1, ..., m\} \mid p_k \leq t(k, m, \alpha)\}.$$

If we now reject the first $H_1, ..., H_{k_{max}(m,\alpha)}$ of our m null hypotheses, we can expect to only falsely reject a fraction of size $\alpha \in [0, 1]$ of these hypotheses. A detailed theoretical treatment of this statistical technique method can be found in the article by Benjamini and Yekutieli [2001] [3].

The programming language `Python` was used to implement the Benjamini-Hochberg-Yekutieli procedure and apply it to our data to select significant edges in our network. In the next section, we will take a closer look at this network.

3 Brain Network Analysis

3.1 Network Structure

In this section, we can finally put all the above methods together to construct a network with the following parameters:

- one node for each of the first $n = 50$ labeled independent components (here enumerated from 0 to 49),
- a time lag of $\tau = 3$ (4.5 seconds),
- an empirical null distribution $\hat{F}_0$ constructed from $\frac{315*314}{2}*300 = 14836500$ values generated via block bootstrapping and
- a false discovery rate for significant edges of $\alpha = 0.4$.

The resulting graph G is depicted in figures 3 and 4. Our method delivered a network with a total number of $n = 50$ nodes and 77 significant edges and its structure is dominated by one big component. An exact list of weighted edges between labeled nodes can be found in Appendix C.

The edges are weighted according to their associated cross-correlation values. There are 55 blue edges that indicate negative correlations ($\mu = -0.1773$, $\sigma = 0.061836$) and 22 red edges that indicate positive correlations ($\mu = 0.169293$, $\sigma = 0.0554999$). We remember, that the direction of an edge can be seen as the direction of time. If there is an edge from node x_i to node x_j, then x_i "happens" 4.5 seconds before x_j and the correlation value between the time-shifted versions of x_i and x_j is significant.

G provides a visualization of the linear time-lagged dependence structure between different cognitive subprocesses and brain areas active during the processing of natural human interaction. We can see that most functional labels are connected to communication and language (social, listening, sound, speech, sentence, word,...).

A natural question to ask is if the topological structure of this graph is in any way "special". Despite the fact that G only has 50 nodes, it consits of 18 disconnected pieces. We can see one big component, G_1 a number of small chain-like pieces and some isolated nodes. Some nodes seem to be hubs and attract more edges than others. It is also eye-catching that there is a total number of 29 self-loops and that most egdes are blue. And what about the density of edges in G and the length of paths between nodes? Are the 77 significant edges randomly distributed among the 50 independent components or do the topological properties of G reflect some inherent non-random biological tendencies of large-scale neural networks?

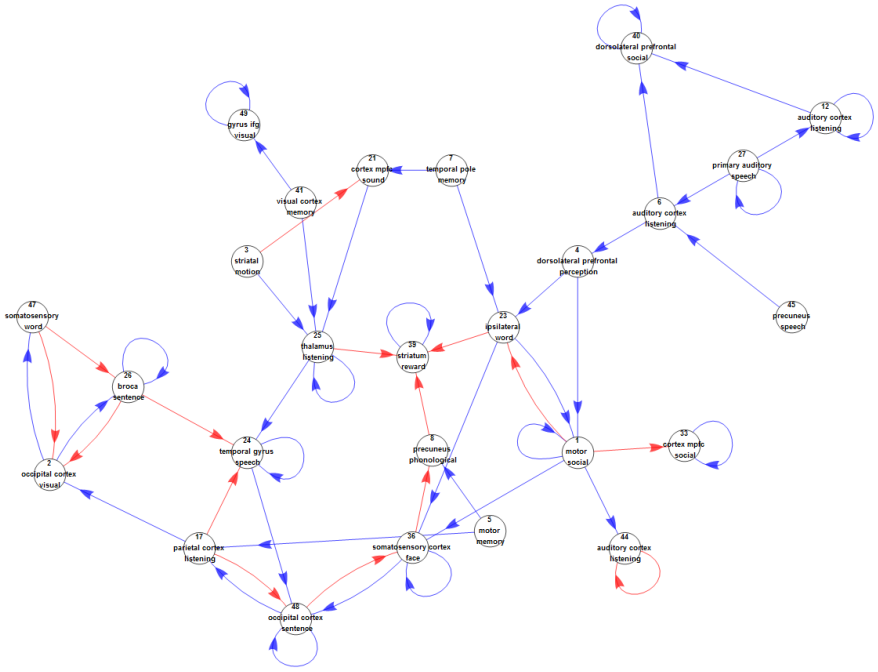

Figure 3: Big weakly connected component G_1 of G (`Wolfram Mathematica`).

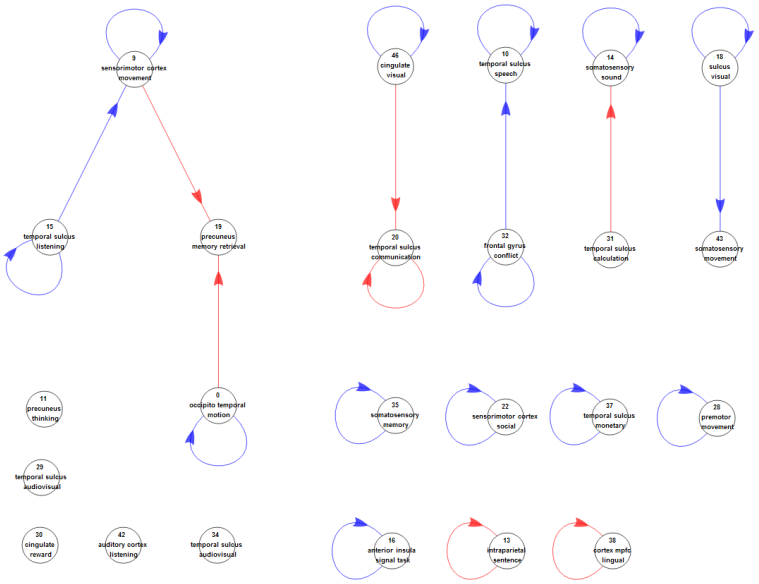

Figure 4: Small weakly connected components of G (`Wolfram Mathematica`).

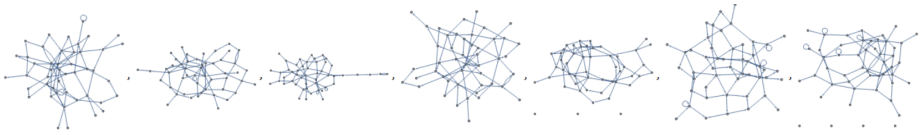

Figure 5: Sequence of random networks $H_1, H_2, ...$ (`Wolfram Mathematica`)

To find a quantitative answer to this question, we used the programming language `Wolfram Mathematica` to simulate a large number of random "null networks" $H_1, ..., H_d$. These networks were used to generate empirical null distributions for different structural network descriptors. Each random network H_i has $n = 50$ nodes and is constructed by randomly and uniformly distributing 77 directed edges among those nodes (including possible self-loops). A sequence of such random networks can be seen in figure 5. We constructed a total number of $d = 100\ 000$ random networks to derived empirical distributions for 6 structural descriptors.

Before we can proceed, we need to introduce some formal definitions concerning network structure. For this purpose, let $N = \{1, ..., n\}$ be the set of nodes of a graph H and let $E \subseteq N \times N$ be the associated set of directed edges of H. Furtermore, for any set A, let $|A|$ be the total number of elements in A.

- **Mean Clustering Coefficient $\mathbf{C_H}$**: Let $i \in N$. Then the set of *neighbours* of i is given by

$$N_i := \{j \in N \mid j \neq i \quad \text{and} \quad (i,j) \in E \quad \text{or} \quad (j,i) \in E\}.$$

  The local clustering coefficient C_i of i in H is defined as the number of all edges between different neighbours of i divided by the number of all *possible* edges between different neighbours of i:

$$C_i := \frac{|\{(j_1, j_2) \in E \mid j_1 \neq j_2 \quad \text{and} \quad j_1, j_2 \in N_i\}|}{|N_i|(|N_i| - 1)}.$$

  If $|N_i| < 2$, then $C_i := 0$. This provides a measure for the density of edges in a neighbourhood of i. The *mean* clustering coefficient of H,

$$C_H := \frac{1}{n} \sum_{i=1}^{n} C_i \in [0, 1],$$

  is the arithmetic mean over all local clustering coefficients and measures the global density of edges in H.

- **Number of Weakly Connected Components $\mathbf{W_H}$**: Imagine we take the graph H and make it a simple graph H_{simple} by transforming the directed set of edges E into a corresponding set of undirected edges

$$E_{\text{simple}} := \{\{i, j\} \mid (i, j) \in E\}.$$

A subset of nodes $M \subseteq N$ is called a connected component of H_{simple} if it is a maximal set such that there is a path between any two nodes in M. If M is a connected component of H_{simple}, we call it a *weakly* connected component of H.

- **Mean shortest weak path length $\mathbf{P_H}$**: Let $i, j \in N$ and $i \neq j$. We say that there is a weak path from i to j in H if there is a path from i to j in H_{simple}. This is equivalent to saying that i and j are in the same weakly connected component of H. We define the mean shortest weak path length of H as the sum of the lengths of the shortest weak paths between all different pairs of weakly linked nodes divided by the number of all different pairs of weakly linked nodes in H. Let $H_1, ..., H_k$ be the weakly connected components of H. Then:

$$P_H := \frac{\sum_{l=1}^{k} \sum_{\{i,j\} \subseteq H_l, i \neq j} \text{Length of Shortest Weak Path between i and j}}{\sum_{l=1}^{k} \frac{|H_l|(|H_l|-1)}{2}}.$$

  If we randomly pick two different nodes $i, j \in N$ that are in the same weakly connected component of H, then the mean shortest weak path length tells us how long we can expect the shortest weak path from i to j to be.

- **Number of Self-Loops $\mathbf{S_H}$**: Let $i \in N$. A self-loop is an edge of the form $(i, i) \in E$.

- **Number of Feedback-Loops $\mathbf{L_H}$**: Let $i, j \in N$. We say that there is a feedback loop between i and j if there is an edge from i to j and an edge from j to i. This means that $(i, j), (j, i) \in E$.

- **Degree of a Node**: Let $i \in N$. The sum of the number of edges leading to i and the number of edges leading away from i is called the degree of i. If i has a self-loop, this increases its degree by 2.

- **Number of Hubs $\mathbf{Z_H}$**: A node $i \in N$ with a degree that is much higher than the degree of most other nodes is called a hub.

For practical reasons, we will here consider nodes with a degree ≥ 7 as hubs. This leaves G with 4 different hubs:

- *(*25 - *thalamus - listening)* (deg = 7),
- *(*48 - *occipital cortex - sentence)* (deg = 7),
- *(*36 - *somatosensory cortex - face)* (deg = 7) and
- *(*1 - *motor - social)* (deg = 8).

In our simulation study, we compared the number of weakly connected components W_G, the number of self-loops S_G, the number of feedback-loops L_G

and the number of hubs Z_G of G with null distributions obtained from random graphs $H_1, ..., H_{100\ 000}$. Furthermore, we compared the clustering coefficient C_{G_1} and mean average weak path length P_{G_1} of the biggest weakly component G_1 of G with the corresponding distributions for the biggest weakly components of our random graphs [3]. As an example, histograms for the distributions of our simulated values for the number of self-loops and the clustering in the biggest component can be seen in figures 6 and 7.

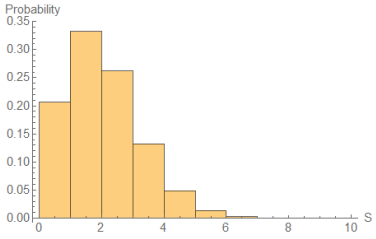

Figure 6: Number of self-loops S_H (`Wolfram Mathematica`).

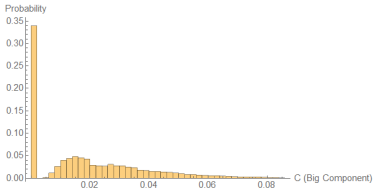

Figure 7: Clustering coefficient of big component C (`Wolfram Mathematica`).

We obtained p-values for G for all 6 structural descriptors from above. Our results are presented in the following table:

Str. Descriptor	**Mean ($\mathbf{H_1, ..., H_{100\ 000}}$)**	**G**	**p-value (G)**
W_G (Components)	3.37404	18	0
S_G (Self-Loops)	1.53971	29	0
L_G (Feedback-Loops)	1.15185	5	0.01136
Z_G (Hubs)	1.67513	4	0.06063
C_{G_1} (Clustering)	0.0197263	0.0910256	0.00533
P_{G_1} (Path-Length)	3.45485	3.6	0.18879

3.2 Interpretation

Per construction, G and every random network H have the same amount of nodes, the same amount of edges and (therefore) the same average node-degree.

[3] Every simulated random graph had one dominating component with at least 35 nodes. The strong tendency to produce giant components at a certain number of edges is well-studied in different classes of random graphs.

But we can see that the structure of our network nevertheless deviates from H in several ways. G shows a significantly higher number of self-loops, feedback loops and weakly connected components. Furthermore, the biggest weakly connected component of G has a significantly higher clustering coefficient than the corresponding biggest weakly connected component of H. The mean shortest weak path length in the biggest component and the number of hubs, on the other hand, do not seem to be higher than in the random case. Here we speculate about possible interpretations of these findings.

- If we take a look at G, we can see that almost all self-loops are blue edges and therefore correspond to negative cross correlation values. This could indicate a tendency of certain brain regions like *(25 - thalamus - listening)*, *(12 - auditory cortex - listening)* and *(48 - occipital cortex - sentence)* to show oscilattory behaviour in their activity. And indeed, many large- and small-scale neuronal networks are known to exhibit periodicity in their activity patterns. In particular, the Thalamus and several regions in the Cortex are known to show oscillatory behaviour [13].

- We could show a significantly increased number of feedback loops in G. Furthermore, all of these feedback loops consist of exactly one blue and one red edge. This is yet another structural property that could be caused by a form of oscillating behaviour. To illustrate this idea, let us assume that we have a blue edge from A to B, a red edge from B to A and that both edges indicate perfect linear dependence. If we start in an initial state where both A and B have a below-average activity level, then after τ time units, A is still below average, but B is above average. After another τ units of time, A and B are both above average. After the next step, A is still above average but B is below average. And after step 4, both A and B are below average again.

- It seems reasonable, that the increased number of weakly connected components in G is (at least partly) caused by the tendency for its nodes to form self-loops and the limited number of edges due to our strict significance analysis. A higher number of self-loops means that there are less edges availabe to link together disconnected components.

- The properties of a graph to have a significantly increased clustering coefficient but a normal average path length when compared to an equivalent random graph have been used to quantify the structural quality of *small-worldness*. A small world graph typically consists of local communities of densely linked nodes that are efficiently connected by short paths. Small-world graphs can be found among a wide range of fields, including social network analysis, logisitics and biology. Humphries et. al. [2006] [9] could detect small-world structures in neural networks found in vertebratebrains. Their result shows parallels to the findings in our project. Though one should note that when computing the clustering coefficients and average weak path lengths, we did not focus on the whole graph, but only on

its biggest component. This also implies, that our construction of random graphs differs in some details from the method used by Humphries. Also, small-worldness normally only has strong implications for sufficiently big graphs and is therefore rarely studied in networks as small as G.

Finally, if we again look at the big component G_1, we can see that the groups $B_1 := \{47, 26, 2\}$ (left), $B_2 = \{4, 45, 6, 27, 12, 40\}$ (upper right corner) and $B_3 = \{49, 41\}$ (top) are only losely connected to the main body of G_1. If we take a look at the node-labels, we could speculate that B_1 has to do with speech production, B_2 with listening and B_3 with the processing of visual stimuli. The main body of G_1, on the other hand, contains both nodes labeled with *motor* as well as the labels *striatum* and *striatal*. Could it be possible to split up the network into functional subgraphs and in the process discover an underlying core-periphery structure as it was found by Bassett et. al. [2013] [1] in individuals learning a new motor skills? In our study, the core-periphery structure of G_1 was not explicit enough to be rigorously quantified, which could partly be due to the small network size. Nevertheless, future research in this direction with more available data seems to be promising.

3.3 Further Thoughts

The above project has demonstrated the possibility to explore the working mechanisms of cognitive processing of real-life human interaction via network analysis of fMRI data. We could see that brain networks constructed via cross-correlation of activity time series of different subregions of the brain differ significantly in several topological aspects from equivalent random networks.

In the above interpretations, though, we should not fully exclude the possibility that the structure of G, to a certain extent, reflects structural details of the experimental stimulus that do not generalize to other situations in which the brain is processing natural human interaction. For example, the properties of G that suggest oscilating behaviour could be partly caused by oscillations within the experimental stimulus (repetitive patterns in the TV show).

Still, our findings point in the direction of a hidden non-trivial network architecture that the brain uses to orchestrate the interplay of a wide range of mental functions when processing natural stimuli. It seems likely, that oscillation and high clustering are natural features of this architecture.

Future research is necessary in order to better understand the dynamics of brain networks in real-world situations. Is there essentially one network associated with the processing of human interaction that can be found in a wide range of individuals? How big are differences among the networks of different individuals? If there are differences, how can they be explained and how do they relate to individual characteristics? Do the topological properties of the above network dynamically change over time within the same individual? If yes, what factors influence this change? How does the structure of G change for varying stimuli and different communication contexts?

These questions could possibly be answered in the future by investigating the brain using the rigorous quantitative tools of graph theory. The above results are encouraging that network science can deepen our understanding of the detailed working mechanisms of the mind in natural situations

4 Appendixes

4.1 A: Imaging Technique

Brain imaging was performed with a 3 Tesla MR scanner (GE Medical Systems, Milwaukee, WI). Anatomical images were aquired with a volumetric MP-RAGE sequence by using a volumetric MP-RAGE sequence and functional activation maps were superimposed (voxel size = 1.5x0.9x0.9 mm, sagittal slices = 120, FoV = 24). An EPI sequence sensitive to BOLD contrast was used for functional imaging (voxel size = 3.45 x 3.45 x 5, axial slices = 25, FoV = 220, base resolution = 64, TR = 1500 ms, TE = 30 ms, flip angle = 75 deg). Each of the 6 functional runs that were performed during the experiment started with a 10.5 second black screen that faded out. This was done to allow magnetization to converge to a steady state; the images corresponding to the initial black screens were removed from the data.

4.2 B: Data Preprocessing before ICA

The raw experimental time series data data was preprocessed using the `AFNI` software package (Cox, [1996], [6]). Anatomical images were corrected for non-uniformity and intensity. Furthermore, they were skull stripped (Iglesias et. al., [2011], [11]), non-linearly registered to an MNI template and inflated to surface based representations using `Freesurfer` software. This was done to create an anatomical parcellation for later use as regions of interest (Fischl, [2012], [7]).

Spatial registration of the functional images from the six runs in 3D space was done via Fourier transformation. *Spikes* were defined as signal intensities greater than 2.5 standard deviations from the mean and were removed. Slice timing differences were corrected. Then, each run was corrected for head movements by registration to the mean of the middle functional run. Each run was masked to remove voxels outside of the participants brain. Finally, the time series were linearly, quadratically and cubically detrended, normalized (by making the sum-of-squares equal to 1) and concatenated to obtain one long time series.

To free this resulting timeseries from artifacts, it was submitted to independent components analysis (ICA) (Beckmann & Smith,[2004], [2]). In particular, resulting components were automatically labelled as not-artifacts, possible artifacts, or artifacts using `SOCK` (Bhaganagarapu, Jackson, & Abbott, [2014], [4]). Each was manually reviewed for accuracy. There were an average of 237.29 components and an average of 177.79 artifactual components (74.93 %) across participants. The independent component time course associated with each artifactual component was removed from the timeseries at each voxel using linear least squares regression. Finally, blurred the resulting timeseries was blurred to a smoothness of 6 mm (Friedman et. al, [2006], [8]).

4.3 C: List of 77 Weighted Edges of G

- (0 + occipito temporal + motion) => (0 + occipito temporal + motion), weight = -0.165526946117
- (0 + occipito temporal + motion) => (19 + precuneus + memory retrieval), weight = 0.157828446212

- (1 + motor + social) => (1 + motor + social), weight = -0.111552330427
- (1 + motor + social) => (23 + ipsilateral + word), weight = 0.118647553486
- (1 + motor + social) => (33 + cortex mpfc + social), weight = 0.194664091054
- (1 + motor + social) => (36 + somatosensory cortex + face), weight = -0.112434737389
- (1 + motor + social) => (44 + auditory cortex + listening), weight = -0.148694333574
- (2 + occipital cortex + visual) => (26 + broca + sentence), weight = -0.121056445465
- (2 + occipital cortex + visual) => (47 + somatosensory + word), weight = -0.232245570409
- (3 + striatal + motion) => (21 + cortex mpfc + sound), weight = 0.121028379295
- (3 + striatal + motion) => (25 + thalamus + listening), weight = -0.136624723336
- (4 + dorsolateral prefrontal + perception) => (1 + motor + social), weight = -0.204862759361
- (4 + dorsolateral prefrontal + perception) => (23 + ipsilateral + word), weight = -0.111180730092
- (5 + motor + memory) => (8 + precuneus + phonological), weight = -0.124787878431
- (5 + motor + memory) => (17 + parietal cortex + listening), weight = -0.130759206722
- (6 + auditory cortex + listening) => (4 + dorsolateral prefrontal + perception), weight = -0.347654521487
- (6 + auditory cortex + listening) => (40 + dorsolateral prefrontal + social), weight = -0.141611723934
- (7 + temporal pole + memory) => (21 + cortex mpfc + sound), weight = -0.197987395627
- (7 + temporal pole + memory) => (23 + ipsilateral + word), weight = -0.137834525273
- (8 + precuneus + phonological) => (39 + striatum + reward), weight = 0.14827338962
- (9 + sensorimotor cortex + movement) => (9 + sensorimotor cortex + movement), weight = -0.167713130731
- (9 + sensorimotor cortex + movement) => (19 + precuneus + memory retrieval), weight = 0.141508472172
- (10 + temporal sulcus + speech) => (10 + temporal sulcus + speech), weight = -0.222638514632
- (12 + auditory cortex + listening) => (12 + auditory cortex + listening), weight = -0.167077347585
- (12 + auditory cortex + listening) => (40 + dorsolateral prefrontal + social), weight = -0.113859753102
- (13 + intraparietal + sentence) => (13 + intraparietal + sentence), weight = 0.142402502181
- (14 + somatosensory + sound) => (14 + somatosensory + sound), weight = -0.238293838284
- (15 + temporal sulcus + listening) => (9 + sensorimotor cortex + movement), weight = -0.192235306613
- (15 + temporal sulcus + listening) => (15 + temporal sulcus + listening), weight = -0.11177298567
- (16 + anterior insula + signal task) => (16 + anterior insula + signal task), weight = -0.200486249759
- (17 + parietal cortex + listening) => (2 + occipital cortex + visual), weight = -0.193487867633
- (17 + parietal cortex + listening) => (24 + temporal gyrus + speech), weight = 0.109474501992
- (17 + parietal cortex + listening) => (48 + occipital cortex + sentence), weight = 0.113666120812
- (18 + sulcus + visual) => (18 + sulcus + visual), weight = -0.233146876166
- (18 + sulcus + visual) => (43 + somatosensory + movement), weight = -0.28446704876
- (20 + temporal sulcus + communication) => (20 + temporal sulcus + communication), weight = 0.155626507705
- (21 + cortex mpfc + sound) => (25 + thalamus + listening), weight = -0.230860457176
- (22 + sensorimotor cortex + social) => (22 + sensorimotor cortex + social), weight = -0.161929353887
- (23 + ipsilateral + word) => (1 + motor + social), weight = -0.16042572092
- (23 + ipsilateral + word) => (36 + somatosensory cortex + face), weight = -0.106482445042
- (23 + ipsilateral + word) => (39 + striatum + reward), weight = 0.13063848065
- (24 + temporal gyrus + speech) => (24 + temporal gyrus + speech), weight = -0.120301391877

- (24 + temporal gyrus + speech) => (48 + occipital cortex + sentence), weight = -0.141623673619
- (25 + thalamus + listening) => (24 + temporal gyrus + speech), weight = -0.234965063953
- (25 + thalamus + listening) => (25 + thalamus + listening), weight = -0.117895222726
- (25 + thalamus + listening) => (39 + striatum + reward), weight = 0.155196237005
- (26 + broca + sentence) => (2 + occipital cortex + visual), weight = 0.145349615846
- (26 + broca + sentence) => (24 + temporal gyrus + speech), weight = 0.124309883636
- (26 + broca + sentence) => (26 + broca + sentence), weight = -0.164852427138
- (27 + primary auditory + speech) => (6 + auditory cortex + listening), weight = -0.143612560657
- (27 + primary auditory + speech) => (12 + auditory cortex + listening), weight = -0.304697127702
- (27 + primary auditory + speech) => (27 + primary auditory + speech), weight = -0.245148685934
- (28 + premotor + movement) => (28 + premotor + movement), weight = -0.24424198595
- (31 + temporal sulcus + calculation) => (14 + somatosensory + sound), weight = 0.226760207461
- (32 + frontal gyrus + conflict) => (10 + temporal sulcus + speech), weight = -0.3712928888
- (32 + frontal gyrus + conflict) => (32 + frontal gyrus + conflict), weight = -0.197211165172
- (33 + cortex mpfc + social) => (33 + cortex mpfc + social), weight = -0.189655221104
- (35 + somatosensory + memory) => (35 + somatosensory + memory), weight = -0.200502186579
- (36 + somatosensory cortex + face) => (8 + precuneus + phonological), weight = 0.118770611062
- (36 + somatosensory cortex + face) => (36 + somatosensory cortex + face), weight = -0.159607963778
- (36 + somatosensory cortex + face) => (48 + occipital cortex + sentence), weight = -0.209993748056
- (37 + temporal sulcus + monetary) => (37 + temporal sulcus + monetary), weight = -0.256670485105
- (38 + cortex mpfc + lingual) => (38 + cortex mpfc + lingual), weight = 0.288168438788
- (39 + striatum + reward) => (39 + striatum + reward), weight = -0.111318523818
- (40 + dorsolateral prefrontal + social) => (40 + dorsolateral prefrontal + social), weight = -0.173041090774
- (41 + visual cortex + memory) => (25 + thalamus + listening), weight = -0.147455098201
- (41 + visual cortex + memory) => (49 + gyrus ifg + visual), weight = -0.107876773272
- (44 + auditory cortex + listening) => (44 + auditory cortex + listening), weight = 0.157567408365
- (45 + precuneus + speech) => (6 + auditory cortex + listening), weight = -0.112320015576
- (46 + cingulate + visual) => (20 + temporal sulcus + communication), weight = 0.256881341245
- (46 + cingulate + visual) => (46 + cingulate + visual), weight = -0.107942124615
- (47 + somatosensory + word) => (2 + occipital cortex + visual), weight = 0.249064800993
- (47 + somatosensory + word) => (26 + broca + sentence), weight = 0.193581854477
- (48 + occipital cortex + sentence) => (17 + parietal cortex + listening), weight = -0.143402140416
- (48 + occipital cortex + sentence) => (36 + somatosensory cortex + face), weight = 0.275030232774
- (48 + occipital cortex + sentence) => (48 + occipital cortex + sentence), weight = -0.125190591306
- (49 + gyrus ifg + visual) => (49 + gyrus ifg + visual), weight = -0.211014151495

References

[1] Danielle S Bassett, Nicholas F Wymbs, M Puck Rombach, Mason A Porter, Peter J Mucha, and Scott T Grafton. Task-based core-periphery organization of human brain dynamics. *PLoS Comput Biol*, 9(9):e1003171, 2013.

[2] Christian F Beckmann and Stephen M Smith. Probabilistic independent component analysis for functional magnetic resonance imaging. *IEEE transactions on medical imaging*, 23(2):137–152, 2004.

[3] Yoav Benjamini and Daniel Yekutieli. *Annals of statistics*, pages 1165–1188, 2001.

[4] Kaushik Bhaganagarapu, Graeme D Jackson, and David F Abbott. Denoising with a sock can improve the performance of event-related ica. *Frontiers in neuroscience*, 8, 2014.

[5] Cécile Bordier, Michel Dojat, and Pierre Lafaye de Micheaux. Temporal and spatial independent component analysis for fmri data sets embedded in the analyzefmri r package. *Journal of Statistical Software*, 44(9):1–24, 2011.

[6] Robert W Cox. Afni: software for analysis and visualization of functional magnetic resonance neuroimages. *Computers and Biomedical research*, 29(3):162–173, 1996.

[7] Bruce Fischl. Freesurfer. *Neuroimage*, 62(2):774–781, 2012.

[8] Lee Friedman, Gary H Glover, Diana Krenz, Vince Magnotta, and The FIRST BIRN. Reducing inter-scanner variability of activation in a multicenter fmri study: role of smoothness equalization. *Neuroimage*, 32(4):1656–1668, 2006.

[9] Mark D Humphries, Kevin Gurney, and Tony J Prescott. The brainstem reticular formation is a small-world, not scale-free, network. *Proceedings of the Royal Society of London B: Biological Sciences*, 273(1585):503–511, 2006.

[10] Aapo Hyvärinen and Erkki Oja. Independent component analysis: algorithms and applications. *Neural networks*, 13(4):411–430, 2000.

[11] Juan Eugenio Iglesias, Cheng-Yi Liu, Paul M Thompson, and Zhuowen Tu. Robust brain extraction across datasets and comparison with publicly available methods. *IEEE transactions on medical imaging*, 30(9):1617–1634, 2011.

[12] Jeremy I Skipper. The nolb model: A model of the natural organization of language and the brain. *Cognitive Neuroscience of Natural Language Use*, pages 101–134, 2015.

[13] Mircea Steriade, David A McCormick, and Terrence J Sejnowski. Thalamocortical oscillations in the sleeping and aroused brain. *SCIENCE-NEW YORK THEN WASHINGTON-*, 262:679–679, 1993.

[14] Martijn P van den Heuvel, Cornelis J Stam, René S Kahn, and Hilleke E Hulshoff Pol. Efficiency of functional brain networks and intellectual performance. *Journal of Neuroscience*, 29(23):7619–7624, 2009.

[15] Tal Yarkoni, Russell A Poldrack, Thomas E Nichols, David C Van Essen, and Tor D Wager. Large-scale automated synthesis of human functional neuroimaging data. *Nature methods*, 8(8):665–670, 2011.

List of Figures

1 Activity time series of temporal independent component (`Python`). 6
2 Empirical distribution $\hat{F}_0$, constructed from 14 836 500 realizations of K_0 (`Python`). 11
3 Big weakly connected component G_1 of G (`Wolfram Mathematica`). 14
4 Small weakly connected components of G (`Wolfram Mathematica`). 14
5 Sequence of random networks $H_1, H_2, ...$ (`Wolfram Mathematica`) 15
6 Number of self-loops S_H (`Wolfram Mathematica`). 17
7 Clustering coefficient of big component C (`Wolfram Mathematica`). 17